Applied Physics Letters

Any-polar resistive switching behavior in LATP films

Cite as: Appl. Phys. Lett. **115**, 143506 (2019); https://doi.org/10.1063/1.5114860
Submitted: 13 June 2019 . Accepted: 16 September 2019 . Published Online: 02 October 2019

J. L. Jiao, L. C. Li, S. Cheng, A. L. Chang, Y. C. Mao, W. Huang, J. Y. Wang, J. F. Xu, J. Li, C. Li, and S. Y. Chen

Applied Physics Letters ARTICLE scitation.org/journal/apl

Any-polar resistive switching behavior in LATP films

Cite as: Appl. Phys. Lett. **115**, 143506 (2019); doi: 10.1063/1.5114860
Submitted: 13 June 2019 · Accepted: 16 September 2019 ·
Published Online: 2 October 2019

J. L. Jiao, L. C. Li, S. Cheng, A. L. Chang, Y. C. Mao, W. Huang,[a] J. Y. Wang, J. F. Xu, J. Li, C. Li, and S. Y. Chen

AFFILIATIONS

Department of Physics and Jiujiang Research Institute, Xiamen University, Xiamen 361005, People's Republic of China

[a]E-mail: weihuang@xmu.edu.cn

ABSTRACT

We demonstrate the coexistence and conversion of the unipolar and bipolar resistive switching behavior in Pt/$Li_{1+x}Al_xTi_{2-x}(PO_4)_3$ (LATP)/Pt structures fabricated by sputtering. The dielectric constant (k) of the LATP film equals 12.0. After the electroforming, the Pt/LATP/Pt resistive switching device exhibits either unipolar switching mode (URS) or bipolar switching mode (BRS). The switching mode can be freely converted between URS and BRS with the same compliance current. This will provide a foundation for a switching mode called any-polar switching mode. The switching mechanism is believed to be related to the formation and rupture of conductive filaments and the excellent oxygen storage capacitance of the LATP film.

Recently, resistive random access memory (RRAM) has been considered to be one of the most promising candidates for next-generation nonvolatile memory due to its simple structure,[1] subnanosecond operation speed,[2,3] low power consumption,[4,5] high density, high-endurance,[6] and complementary metal-oxide-semiconductor (CMOS) compatibility.[7] The resistance is switched between a high-resistance state (HRS or OFF state) and a low-resistance state (LRS or ON state), driven by an applied voltage bias. This bias-tuned resistance reducing phenomenon is also called negative resistance in early literature studies on metal-insulator-metal diodes.[8–10] The switching event from the HRS to the LRS and the corresponding voltage are denoted as SET operation and V_{SET}, respectively. In contrast, the switching event from the LRS to the HRS and the corresponding voltage are denoted as RESET operation and V_{RESET}, respectively. Current compliance is commonly required in the electroforming and the SET operations to avoid permanent breakdown. There are two types of switching modes which are unipolar switching mode (URS) and bipolar switching mode (BRS). The former requires the same electrical polarity during the SET and RESET operations, whereas the latter requires opposite electrical polarities.[11] In the past few decades of RRAM research, URS has been mainly observed in devices when using noble metal as both counter electrodes,[12–16] and BRS is mainly observed when one of the electrodes was replaced by oxidizable materials.[17–21]

Interestingly, the conversion between the URS and BRS modes was also studied in several reports on devices with structures of Pt/TiO_2/Pt, Ag/ZnO/Ag, Ni/NiO/Ni, and Pt/$NiFeO_4$: Ag/Pt by Jeong *et al.*[22–30] Some of the conversions are controlled by tuning the compliance current.[22,23,25] Once I_C was increased, the conversion from BRS to URS was found to be irreversible. Some conversions are reversible, and the HRS/LRS currents of both modes are comparable.[24,26,28,30] But the switching voltages include V_{SET} and V_{RESET} which are different and irrelevant when comparing the two modes. However, in our case of $Li_{1+x}Al_xTi_{2-x}(PO_4)_3$ (LATP), the V_{SET} and V_{RESET} values are nearly the same for both modes.

A great many materials have been explored as storage media for RRAM. The most reported are binary oxides, ternary oxides, and other complex oxides. However, studies on solid electrolytes as storage media are rarely reported in the literature. $Li_{1+x}Al_xTi_{2-x}(PO_4)_3$ (LATP) has been reported previously in lithium batteries with a natrium super ionic conductor type (NASICON-type) solid electrolyte by Aono *et al.*[31–33] This NASICON-type structure of LATP is formed by the connection of octahedrons and tetrahedrons through oxygen atoms and thus has many crystalline channels.[33] These channels can provide fast transport routes and storage sites for both lithium and oxygen ions. Therefore, it is beneficial to apply LATP as the switching layer in RRAM devices.

In this study, a structure of the Pt/LATP/Pt is fabricated by sputtering. The coexistence of unipolar and bipolar resistive switching modes was found in the Pt/LATP/Pt device, and the conversion capability between the two modes was investigated. The crystalline structure and surface morphology of the LATP thin film were characterized using X-ray diffraction (XRD) and atomic force microscope (AFM).

Auger electron spectroscopy (AES) was used to review the elemental distribution of the LATP on the Pt-substrate.

First, according to the composition of LATP,[21] Li_2CO_3, Al_2O_3, TiO_2, and $NH_4H_2PO_4$, powders were mixed well at the molar ratio of 3.5:1:8:15 and annealed at 800 °C for 2 h in a tube furnace. The annealed process was repeated twice to generate a purer LATP powder. From the annealed powders, a LATP sputtering target was produced by the conventional cold-pressing method. The target was finally sintered at 900 °C for 5 h in a tube furnace in order to obtain a uniform crystal grain size and compactness.

With the LATP target, 20-nm-thick LATP films were RF sputtered on a Pt-substrate [Pt(100 nm)/Ti/n-Si(100)] at 100 W. The Pt-substrate is used as a bottom electrode for the final RRAM device. After LATP film deposition, 100-nm-thick Pt top electrodes with diameters of 800 μm were deposited by DC magnetron sputtering through a mechanical mask. The resistive switching characteristics of the Pt/LATP/Pt RRAM devices were measured using a Keithley 4200 semiconductor parameter analyzer with the Pt top electrode biased and the Pt bottom electrode grounded. The resistive switching measurement was actually carried out in ambient air in this work.

The crystalline structural identification was performed by XRD. Figure 1(a) represents the XRD pattern of the LATP powder, which clearly contains sharp diffraction peaks which symbolize the NASICON structure of $LiTi_2(PO_4)_3$. But as shown in Fig. 1(b), no diffraction peak other than the bottom Pt and Ti peaks is detected from the 20-nm-thick LATP films, which suggests that the room-temperature deposited LATP film is amorphous. AFM characterization of the LATP film revealed an RMS roughness of 1.55 nm in an area of $10 \times 10\ \mu m^2$ [Fig. 1(c)].

To further characterize the element distribution and composition of the LATP film, Fig. 1(d) shows the AES data of the thin films on the Pt-substrate. All the AES elemental depth profiles consist of elements of Li, Al, Ti, P, O, and Pt. With the AES data, the LATP film shows a homogeneous elements distribution and an average composition of the LATP film is $Li_{4.3}Al_{1.1}Ti_{2.5}P_{3.0}O_{11.0}$.

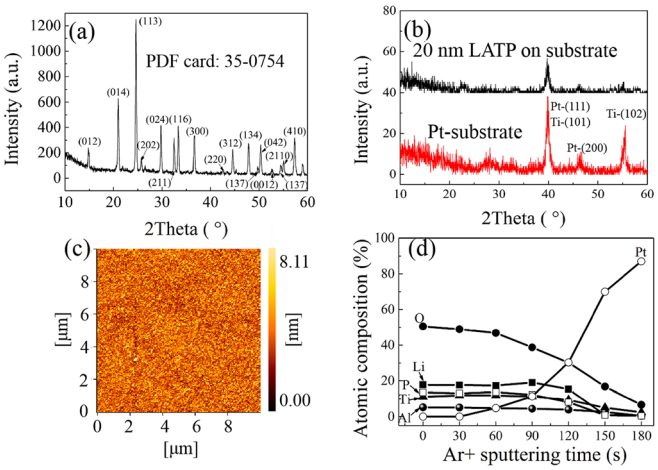

FIG. 1. (a) XRD pattern of LATP powder which made the target; (b) XRD pattern of the 20-nm-thick LATP film; the red line represents the Pt-substrate, and the black line represents the LATP film on the Pt-substrate; (c) AFM image of the LATP film on the Pt-substrate; (d) AES elemental depth profile of the as-deposited LATP film on the Pt-substrate.

In order to evaluate the dielectric constant (k) of the LATP film, a device with a structure of Pt/LATP(20 nm)/n-Si(100)/Al is fabricated on the Si(100) wafer. The diameter of the round Pt top electrode is 600 μm. Figure 2 shows the capacitance voltage curve of the capacitance. The dielectric constant is calculated as high as 12.0, indicating that the LATP film can be a good dielectric.

Figure 3(a) shows a schematic diagram of the fabricated Pt/LATP/Pt RRAM device. Typical current–voltage (I–V) curves of the Pt/LATP/Pt RRAM are plotted on a semilogarithmic scale shown in Figs. 3(b) and 3(c), demonstrating the coexistence of URS and BRS behaviors at room temperature. Both modes were activated after an electroforming process with a compliance current (I_C) of 1 mA. I_C is an essential protection to avoiding the entire hard breakdown of the devices. After electroforming, SET and RESET operations were carried out at opposite polarity (positive RESET and negative SET), leading to the BRS mode, as shown in Fig. 3(b). When the RRAM cell finished 50 cycles in BRS mode, the operation mode was changed to URS, in which both the abrupt RESET and SET operations occurred with positive biases as shown in Fig. 3(c).

We observed that both the positive V_{SET} in URS mode and the negative V_{SET} in BRS mode are around 1.5 V. The V_{RESET} voltages are all around 0.5 V. So we count all the $|V_{SET}|$ absolute and the V_{RESET} of the different switching mode in Fig. 3(d). From the statistics, it is found that the V_{RESET} values distributed between 0.4 and 0.9 V and the $|V_{SET}|$ values varied from 1.2 to 2.3 V. Figure 3(e) represents the distribution of the resistances read at ±0.2 V during the successive switching cycles of the LATP device. The LRS and the HRS exhibit good uniformity. No overlap of the LRS and HRS resistances occurs even after the many switching cycles, and the LRS resistance tends to be even more stable as the number of loops increases. The calculated resistance ratio of HRS to LRS is higher than 200.

To investigate the device-to-device uniformity of the resistive switching property, we randomly selected six devices and characterized the HRS/LRS resistances. As shown in Fig. 3(f), stable HRS/LRS resistances contribute an average HRS/LRS ratio of 10^3.

To further investigate the conversion capability, special cyclic tests which cycled between the URS and BRS modes were performed on the Pt/LATP/Pt device. As displayed in Fig. 4(a), the conversion

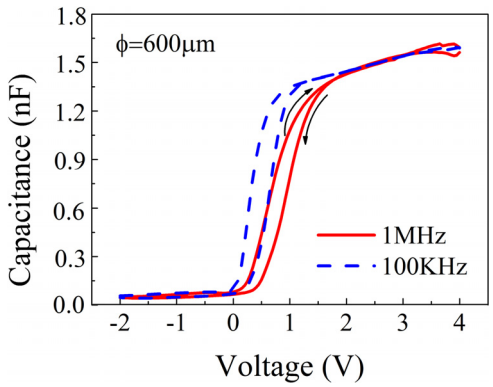

FIG. 2. Capacitance-voltage curve of the Pt/LATP/n-Si/Al capacitance.

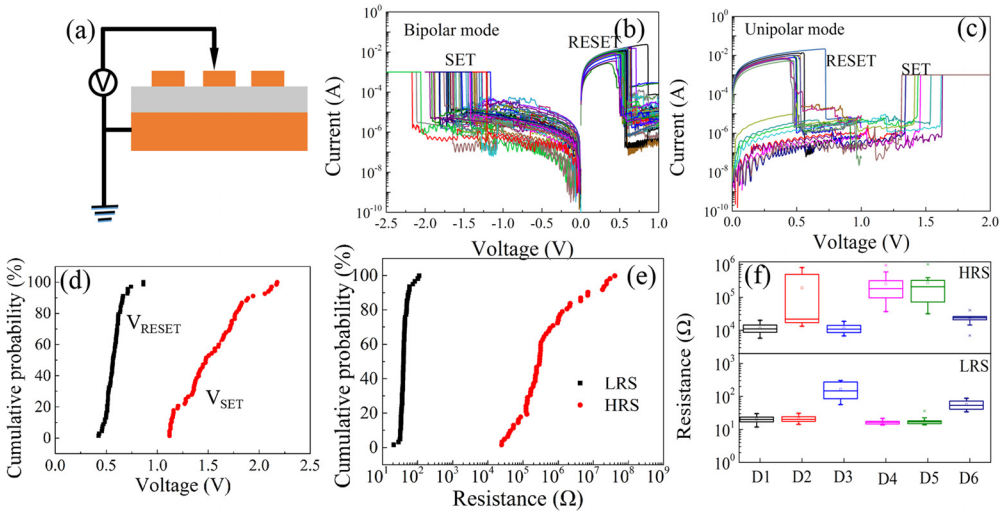

FIG. 3. (a) Schematic diagram of the Pt/LATP/Pt RRAM device and the electrical measurement configuration; Typical I–V characteristic of the LATP RRAM performed in (b) BRS mode and (c) URS mode; Statistical distribution of the RRAM cell: (d) SET and RESET voltages and (e) HRS/LRS resistances; (f) Distribution of device-to-device HRS/LRS resistances for six randomly selected devices.

test started with URS mode and a constant I_C of 1 mA favored all the cycling loops. The test sequence is on the order of (1)(2)→(2)(3)→(3)(4)→(4)(1)→(1)(2) in which the four switching processes, namely, (1)(2),(2)(3), (3)(4), and (4)(1), can be classified into two URS and two BRS processes. The device was cycled 5–10 times in each process and then transformed to the next process following the above order. Altogether, 75 cycles are shown in Fig. 4(a). The HRS and LRS resistances during the test are depicted in Fig. 4(b), the V_{SET} and V_{RESET} value distributions are shown in Fig. 4(c), and the obtained four operation threshold voltage are positive V_{SET}, negative V_{SET}, positive V_{RESET}, and negative V_{RESET}. Figure 4(d) shows another conversion test which began from BRS mode and followed the process sequence of (1)(4)→(4)(3)→(3)(2)→(2)(1)→(1)(4). Figure 4(e) shows the resistance evolution during the cyclic test of Fig. 4(d), and the ratio of HRS/LRS resistances is generally higher than 100. The corresponding switching voltage distributions are analyzed in Fig. 4(f). When comparing the voltages in Figs. 4(c) and 4(f), no obvious difference is observed, confirming the robust conversion ability which is found to be independent of the switching operation history.

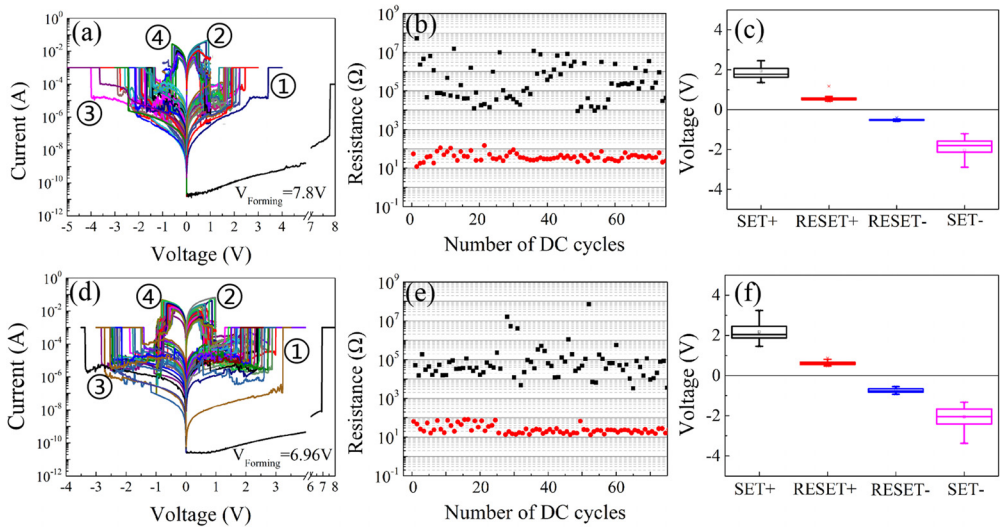

FIG. 4. Conversion test of the Pt/LATP/Pt device between the URS and BRS switching modes: (a) beginning with URS and (d) beginning with BRS. (b) and (e) Evolution of LRS and HRS resistances for the switching cycles in (a) and (d), respectively. The resistances were evaluated at ±0.2 V. (c) and (f) Statistical switching SET and RESET voltages for the switching cycles in (a) and (d), respectively.

The conversion test showed that the Pt/LATP/Pt RRAM device can work in both BRS and URS switching modes. Each mode can be operated at any polar of the bias and seemed to be irrelevant of the initial switching mode and the operation history. Considering the similar HRS and LRS resistances, the similar V_{SET} and V_{RESET} voltages, and the robust conversion/switching ability, the above operation mode is not only different from the conventional URS and BRS mode but also different from most of the previously reported URS/BRS convertible property as summarized above. The previously reported URS/BRS conversions are either irreversible or of poor endurance. Based on our LATP device and the unique operation mode, the amplitude rather than the polarity of the bias is concluded as the key determining factor to switch the device. So the device can be called any-polar resistive memory. A schematic figure of the operations of an ideal any-polar resistive memory is shown in Fig. 5.

In a previous study on the coexistence of the URS and BRS switching, tiny conducting filaments composed of oxygen vacancies or Ag atoms are utilized to explain the LRS states. The Joule heating is believed to breakdown the conduction filaments in URS,[23,24] while in BRS, migration of the oxygen ions (and the corresponding oxygen vacancies or the Ag ions) under an applied electric field is supposed to the dominant mechanism to disconnect the filaments.[25–27,30]

When using noble metal as both counter electrodes, the oxide-based RRAM usually works in URS mode and is confronted by many problems such as instability of operation parameters and unsatisfactory switching endurance. To solve the problem, a thin oxygen gathering layer is necessary to improve the device endurance as in the previously reported TiN/Ti/HfO_x/TiN.[34] But after Ti layer insertion, the device would no longer work in URS mode. The polarity of the BRS of such devices is rigid since only under positive bias can the oxygen ions be gathered by the gettering layer. Otherwise, some of the mobile oxygen ions may vanish into the environment, causing the device to break down.

In the device of Pt/LATP/Pt, the sandwich structure is simple without introducing any oxygen gathering interlayer. However, the BRS switching property is proved to be robust. Furthermore, the polarity of the BRS seems to be reversible. This is quite different from conventional BRS typed RRAM. We may consider the special crystalline structure of the LATP itself. In a crystallized LATP, the lattice structure consists of PO_4 tetrahedrons sharing corners with TiO_6 octahedrons and forming open channels that act as conduction paths for ions including Li^+ and probably O^{2-}. Even when the LATP is deposited in amorphous phases, the conduction paths are retained by the short-range order property of the atoms in solid. The paths not only provide fast moving routes for ions but also act as an oxygen reservoir. Because the oxygen can be stored at any depth of the LATP layer, the BRS switching operation of the Pt/LATP/Pt device is then becoming polarity independent. This means that the BRS can be operated with positive SET and negative RERET or with negative SET and positive RERET. Both are stable operations. The excellent ability to store oxygen in LATP also increased the cycling duration of the URS switches.

Based on the transport and storage ability of the oxygen ions in LATP, a schematic figure of the oxygen ion migration mechanism during the operations of the any-polar LATP resistive switching device is shown in Fig. 5. In the as-fabricated device, oxygen vacancies are randomly distributed in the LATP layer. During the SET operation, a positive or negative bias was applied and the loosely bonded oxygen ions drift against the field, leaving vacancies to form conducting filaments. Then, a subsequent RESET operation can be performed by the Joule heating effect of a large current without compliance or conducted by a reverse bias, which annihilates the vacancies by oxygen ion restoration. The above two effects can contribute to the RESET operation since the RESET current level and the V_{RESET} voltage amplitude are observed to be similar for both bias polarities. According to the detailed oxygen storage part in the LATP layer and the spreading direction of the filaments, the LRS state is discriminated into LRS+ and LRS− states. Based on the operation history, the HRS state is discriminated into HRS+ and HRS− states. Therefore, combinations of the (1)(2) operations and the (3)(4) operations are URS switches, while combinations of the (2)(3) operations and the (4)(1) operations are URS switches.

To analyze the current conduction mechanism of the switching cycles, the I–V curve in Fig. 4(a) under the positive bias is logarithmically redrawn in Fig. 6. An Ohmic behavior was observed in the LRS I–V lines with a slope close to 1 (average slope = 0.95) which is typical for the current conduction in filaments. For the HRS I–V curves, the low voltage (<1 V) part exhibits linear behavior which is again governed by the Ohmic law (average slope = 0.94). But at high voltages

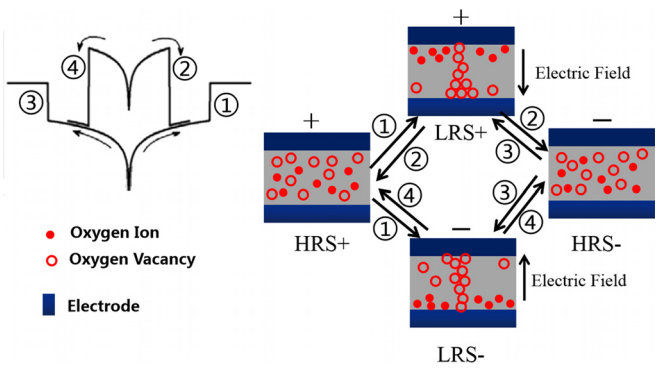

FIG. 5. Schematic description of the resistive switching mechanism of the LATP device.

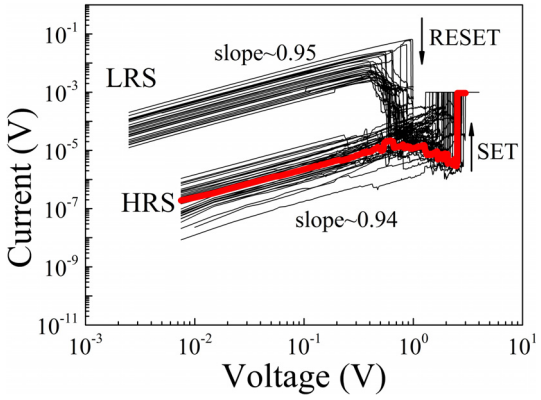

FIG. 6. Logarithmical plot of the HRS and LRS in positive bias from Fig. 4(a); the red line represents a typical I–V curve of the LATP device in HRS.

(>1 V), the current is frequently found to decrease with the increasing bias, see the red line shown in Fig. 6. This phenomenon also occurs in the negatively biased range [as shown in Figs. 4(a) and 4(d)]. All the classic models including space charge limited conduction (SCLC),[35] Schottky emission,[36] and Poole–Frenkel emission[37] never predicted such an unusual behavior. So the fundamental properties of the LATP material were reexamined. It is realized that LATP was traditionally studied as solid electrolyte in lithium batteries for its superior Li^+ conduction ability. It is no doubt that Li^+ is faster moving species than O^{2-} when under bias. So before the bias reached V_{SET} which indicates intense O^{2-} movements, early migration of lithium ions has occurred. From the I–V characteristics, it is found that the electric field for the SET operation is about 1.0×10^6 V/cm, while the significant movement of Li^+ has occurred with a weak electric field of 0.5×10^6 V/cm. Once the Li^+ ions redistributed themselves along the depth of the LATP layer, the appended electric field could counteract the applied electric field bias and lowered the conduction current. However, once the device is switched to LRS by oxygen vacancy filaments, Li+ no longer affects the currents.

In summary, the coexistence and conversion of unipolar and bipolar switching behaviors are demonstrated in the device of Pt/LATP/Pt. The conversion of the URS and BRS was freely conducted without altering the compliance current. The switching voltage and current were also confirmed to be of the same level. As a result, the SET and RESET operations can be performed at any polarity. Then, the Pt/LATP/Pt device can be categorized as a type of resistive memory which is called any-polar RRAM. The any-polar RRAM is expected to find its unique application in future nonvolatile memory.

The authors gratefully acknowledge financial support from the Natural Science Foundation of China (No. 61474094), the National Key Research and Development Program of China (No. 2018YFB2200103), and the weapons and equipment preresearch field fund Project (No. 6140721040411).

REFERENCES

[1]H. P. Wang, H. Y. Lee, S. Yu, Y. S. Chen, and Y. Wu, Proc. IEEE **100**, 1951 (2012).
[2]A. C. Torrezan, J. P. Strachan, G. Medeiros-Ribeiro, and R. S. Williams, Nanotechnology **22**, 485203 (2011).
[3]B. J. Choi, A. C. Torrezan, K. J. Norris, F. Miao, and J. P. Strachan, Nano Lett. **13**, 3213 (2013).
[4]C. H. Cheng, C. Y. Tsai, A. Chin, and F. S. Yeh, in IEDM Technical Digest (2010), p. 448.
[5]B. Govoreanu, G. S. Kar, Y.-Y. Chen, V. Paraschiv, and S. Kubicek, in IEDM Technical Digest (2011), p. 729.
[6]M. J. Lee, C. B. Lee, D. Lee, S. R. Lee, M. Chang, J. H. Hur, Y. B. Kim, C. J. Kim, D. H. Seo, S. Seo, U. I. Chung, I. K. Yoo, and K. Kim, Nat. Mater. **10**, 625 (2011).
[7]W. Lee, J. Park, S. Kim, J. Woo, J. Shin, G. Choi, S. Park, D. Lee, E. Cha, B. H. Lee, and H. Huang, ACS Nano **6**(9), 8166–8172 (2012).
[8]J. G. Simmons and R. R. Verderber, Proc. R. Soc. London, Ser. A **301**(1464), 77–102 (1967).
[9]G. Dearnaley, A. M. Stoneham, and D. V. Morgan, Rep. Prog. Phys. **33**, 1129 (1970).
[10]T. W. Hickmott, Thin Solid Films **9**, 431–446 (1972).
[11]F. Pan, S. Gao, C. Chen, C. Song, and F. Zeng, Mater. Sci. Eng. R **83**, 1–59 (2014).
[12]C. Yoshida, K. Tsunoda, H. Noshiro, and Y. Sugiyama, Appl. Phys. Lett. **91**, 223510 (2007).
[13]N. Xu, L. F. Liu, X. Sun, C. Chen, Y. Wang, D. D. Han, X. Y. Liu, R. Q. Han, J. F. Kang, and B. Yu, Semicond. Sci. Technol. **23**, 075019 (2008).
[14]C. Y. Lin, C.-Y. Wu, T. C. Lee, F. L. Yang, and C. Hu, IEEE Electron Device Lett. **28**, 366–368 (2007).
[15]L. Goux, Y. Y. Chen, L. Pantisano, X. P. Wang, G. Groeseneken, M. Jurczak, and D. J. Wouters, Electrochem. Solid State Lett. **13**, G54–G56 (2010).
[16]C. Y. Lin, C. Y. Wu, C. Hu, and T. Y. Tseng, J. Electrochem. Soc. **154**, G189–G192 (2007).
[17]S. Seo, M. J. Lee, D. H. Seo, E. J. Jeoung, and D. S. Suh, Appl. Phys. Lett. **85**, 5655–5657 (2004).
[18]C. Rohde, B. J. Choi, D. S. Jeong, S. Choi, and J. S. Zhao, Appl. Phys. Lett. **86**, 262907 (2005).
[19]W. Y. Chang, Y. C. Lai, T. B. Wu, S. F. Wang, and F. Chen, Appl. Phys. Lett. **92**, 022110 (2008).
[20]Y. M. Kim and J. S. Lee, J. Appl. Phys. **104**, 114115 (2008).
[21]S. J. Park, W. H. Kim, and W. J. Maeng, Microelectron. Eng. **85**(1), 39–44 (2008).
[22]D. S. Jeong, Z. H. Schroeder, and R. Waser, Electrochem. Solid-State Lett. **10**(8), G51–G53 (2007).
[23]S. Lee, H. J. Kim, J. J. Park, and K. J. Yong, J. Appl. Phys. **108**, 076101 (2010).
[24]L. Goux, J. G. Lisoni, M. Jurczak, D. J. Wouters, and L. Courtade, J. Appl. Phys. **107**, 024512 (2010).
[25]D. L. Xu and Y. Xiong, J. Alloys Compd. **584**, 269–272 (2014).
[26]D. Choi and C. S. Kim, Appl. Phys. Lett. **104**, 193507 (2014).
[27]D. L. Xu, Y. Xiong, and M. H. Tang, Appl. Phys. Lett. **104**, 183501 (2014).
[28]A. Hao, M. Ismail, S. He, W. H. Huang, and N. Qin, J. Appl. Phys. **123**, 085108 (2018).
[29]C. D. Cheng, Y. Q. Li, T. Zhang, and Y. C. Fang, J. Appl. Phys. **124**, 152103 (2018).
[30]W. Hu, X. M. Chen, G. H. Wu, Y. T. Lin, N. Qin, and D. H. Bao, Appl. Phys. Lett. **101**, 063501 (2012).
[31]H. Aono and E. Sugimoto, J. Am. Ceram. Soc. **79**, 2786 (1996).
[32]H. Aono, E. Sugimoto, Y. Sadaoka, and N. Imanaka, J. Electrochem. Soc. **136**, 590 (1989).
[33]K. Baris, D. Schroeder, J. I. Brian, and T. V. John, Chem. Mater. **24**, 287–293 (2012).
[34]S. Z. Rahaman, Y. D. Lin, H. Y. Lee, Y. S. Chen, and P. S. Chen, Langmuir **33**, 4654–4665 (2017).
[35]Q. Liu, W. H. Guan, P. Jiang, W. F. Liu, and M. Liu, Appl. Phys. Lett. **92**, 012117 (2008).
[36]Y. T. Chen, T. C. Chang, P. Jiang, J. J. Huang, H. C. Tseng, P. C. Yang, and A. K. Chu, Appl. Phys. Lett. **102**, 043508 (2013).
[37]C. C. Lin, Z. L. Tseng, K. Y. Lo, C. Y. Huang, and C. S. Hong, Appl. Phys. Lett. **101**, 203501 (2012).